Article

Air Pollution with Fine Particles in Closed Parking and Theoretical Studies of the Interaction of Inhaled Particles in Respiratory Tract

Aleksandras Chlebnikovas [1,2,*] and Raimondas Jasevičius [2,3]

1   Institute of Mechanical Science, Faculty of Mechanics, Vilnius Gediminas Technical University, J. Basanavičiaus g. 28, 03224 Vilnius, Lithuania
2   Institute of Environmental Protection, Faculty of Environmental Engineering, Vilnius Gediminas Technical University, Saulėtekio al. 11, 03225 Vilnius, Lithuania
3   Department of Mechanical and Materials Engineering, Faculty of Mechanics, Vilnius Gediminas Technical University, Saulėtekio al. 11, 03225 Vilnius, Lithuania
*   Correspondence: aleksandras.chlebnikovas@vilniustech.lt; Tel.: +370-6369-3865

Abstract: Indoor air quality must be considered important in regards to its possible harmful effects on the human body. Premises such as underground garages, covered car parks and other similar structures remain crucial in assessing the level of air pollution. In such an environment, the main sources of pollution are motor vehicles, emissions from the heating-ventilation-air-conditioning systems of the engineering networks of the joint building, and pollution. When visiting such premises, a person inhales the air, which contains fine particulate matter and a variety of gaseous pollutants harmful to health. The aim of this study is to assess indoor air pollution with fine particulate matter of 0.3–10 μm depending on the nature of the source, aerodynamic parameters in relation to the potential location of a person, and the mechanical behavior of inhaled particles with respiratory tissues. In this work, the interaction of a fine particle with an alveolar cell is theoretically studied when the particle enters the lungs through the human respiratory tract. Based on the results of this study, it would be possible to assess the extent of pollution and the movement or accumulation of particles in the respiratory system.

Keywords: indoor air quality; parking space; fine particulate matter; tissue of respiratory system; alveoli; discrete element method

1. Introduction

There are different types of marking of the size of particles. We use ultrafine particles (UFPs), which are considered in the range of diameters 100 nm < d <10 μm [1]. Here, it is noted that a particle that is less than 100 nm is a nano particle. Humans can inhale such ultrafine and nano particles. Moreover, small particles with a dimeter of 100 nm (or less) can reach the alveoli [2]. Other scientists consider the even larger range of 5–500 nm [3–5] that can reach the alveolar region. One of the dangers to the human respiratory system, especially when a person is in a confined space, is the diesel fuel particle. The diesel exhaust particles can be subdivided as Nucleation Mode Particles, Accumulation Mode Particles, and Coarse Particles [6]. The mentioned 100 nm size particles can be considered as Accumulation Mode Particles [7]. Generally, accumulation mode particles can be considered as carbonaceous soot agglomerates [8]. Conventional 100 nm diesel particle density is 1.77 ($\pm$0.29) g/cm^3 [9]. The Diesel Nucleation Mode Particles were investigated by Filippo and Maricq [10], who analysed particles of a different nature, which have a solid core and remain non-volatile in temperatures above 400 °C.

A vehicle pollution study found that emissions from closed parking lots were about 40% lower compared to curbside parking lots. The local increase in pollutant emissions

is relevant for identifying possible impacts, but the implementation of this practical field measurement is quite complex, and the dynamics of emissions from pollution sources is not well understood [11,12]. Air quality in downtown garages was analyzed by examining the concentrations of 16 US EPA priority polycyclic aromatic hydrocarbons (PAHs) and heavy metals in samples using active biomonitoring. The results showed that instrumental monitoring is suitable for various pollutants; otherwise, active moss biomonitoring requires improvement and is not accurate for an indoor environment. The authors noted that carbon monoxide and PAHs are also important pollutants for assessing negative health impacts, and sampling should be guided by the influence of the air quality [13]. Infrastructural requirements and regulatory challenges of a sustainable urban air mobility ecosystem and insights for the future are given by Takacs and Haidegger [14], who found that vertical take-off and landing vehicles are gradually forming the future of urban mobility, which is similar to the even-paced expansion of ground electric and/or autonomous vehicles.

In a modern urban city, parking spaces naturally increase due to improved traffic conditions. However, the parking lot itself also becomes a source of air pollution. Therefore, urban transport faces a two-fold task. The evaluation of park accessibility based on the improved Gaussian two-step floating catchment area method was investigated by Li et al. [15], who mentioned that the accessibility challenge could be addressed by considering various factors such as adding the number of parking lots. The assessment of traffic-related air emission based on computational fluid dynamics (CFD) and back propagation (BP) neural networks of optimal routes in an urban area were investigated by Ren et al. [16]. They mentioned that people's exposure to traffic-related particulate matter with an aerodynamic diameter of up to 2.5 μm (PM2.5) primarily occurs during commuting, and the wind environment significantly affected pollutant distribution and diffusion. Another study [17] described a numerical model, along with particle transport theory. The flow of pollutants from the vehicle and the level of particles from the space between two opposite pollution sources in the upward direction during the first 30 s were analyzed.

A binary composite was prepared and its application in autotransport exhaust degradation was analyzed by researchers [18]. They mention that their study is vital for treatment exhaust in the future. Investigation [19] presented the dynamic tensile stress-compressive stress behaviour of thermoplastic matrix composite materials reinforced with continuous fibre for automotive damping and anti-vibration structural elements. Continuous fibre reinforced thermoplastic composites have special properties to reduce the consumption and emissions of polluting gases.

In this work, we will try to consider the parking lot as a source of pollution, considering it in various sections, both from the point of view of the movement of air pollution and from the point of view of the entry of pollution particles into the lungs. Exposure to submicron and fine particulate matter has a profound impact on human health in environments such as underground parking, garages and other enclosed vehicle areas. The studies analysed the change in pollution depending on the season. Most of the results show that the exposure limit was exceeded, especially during the warm and hot seasons. It has also been confirmed that natural air exchange in closed areas does not reach the recommended air freshness, resulting in pollution levels most often exceeding air quality standards. According to studies, it is accepted that there is a relationship between the parameters of fine particulate matter size, background value and traffic flow [20,21]. Studies [22] assessed exposure to gaseous air pollutants from walkways and indoor spaces. $PM_{2.5}$ pollution and the $PM_{2.5}/PM_{10}$ ratio were significantly higher in overpasses than in subways.

However, levels of higher particulate fractions such as $PM_{2.5}$–PM_{10} have been elevated in subways. According to the study, inhalation exposure increased with an increase in the time spent in a polluted area by 179–457%. Exposure increases by 15–18% for pedestrians consuming senior food in the area, and exposure increases by 11–37% at maximum pollution levels. The acute impact of polluted air on lungs has adverse effects, especially during childhood. Permanent or additional exposures could exacerbate injury by increasing the risk of early and potentially more severe decline in lung function after the plateau in early

adulthood. Either scenario can result in lung function that is below the threshold for chronic obstructive pulmonary disease in later adulthood. The research group focuses on primary and secondary ambient air pollutants from the combustion of fossil fuel and described in the US EPA ($PM_{2.5}$ and PM_{10}, i.e., particulate matter up to 2.5 μm and 10 μm). Results were reported separately for different time exposures [23].

Studies have shown that workers have a greater decrease in forced expiratory volume in 1 s when working in a diesel bus garage. The negative impact is also felt in the form of symptoms such as coughing or itching, difficulty breathing and wheezing, burning or tearing [24]. The maximum emission is detected more in the semi-cold season (autumn) than in winter. The pollutants were located in the upper part of the research space under natural ventilation conditions. The calculated correlation with humidity was positive, and with temperature it was negative.

From the perspective of air circulation in parking lots, the aim of these studies was to investigate one of the most common enclosed spaces, such as car parks, where pollution is often favourable and the person entering the area is forced to inhale airborne pollutants. Several goals were identified to be performed in this research, the main ones of which are: to carry out experimental studies of microclimatic conditions in real conditions of various parking lots; to obtain and analyze the results of pollution with fine, ultrafine and nano-sized particles at air pollution research sites of parking lots under similar microclimatic conditions; to create a principal model of the distribution of flows at different inflow velocities on the territory of the parking lot, taking into account the position of a closed parking lot user; to perform a numerical simulation of the fine, ultrafine and nano-sized particles interaction with the alveoli and determine the interaction forces and displacement of this particle.

Problem Formulation

Diesel engine exhaust particles (DEPs) are considered ultrafine particles (UFPs). The goal is to elucidate the ability of ultrafine particles (UFPs) to interact with the alveolar cell. The challenge is to describe the model by evaluating the possible influence of surfactant and alveolar fluid on the UFPs interaction. This work uses the definition of fine (d < 100 μm), ultrafine (d < 10 μm), and nano-sized (d < 0.1 μm) particles proposed by Professor Jürgen Tomas [1]. The numerical simulation used in the work is based on his theory of the interaction of ultrafine particles, so the terminology is also preserved [25,26].

In the known literature, no studies have been observed to numerically study the dynamics of UFP interactions in the alveoli, where a descriptive model would estimate the possible deformation during particle-cell interactions. Thus, the presented study is a novelty of the work, and given the importance of emission requirements, such a study makes sense. This study is a continuation of an earlier study on coronavirus interactions in the lungs [27].

Due to the low circulation of air and the high volume of traffic, high concentrations of fine particulate matter are formed in the space of closed parking lots. No studies have been observed in the literature on the analysis of the impact of very fine and fine particulate matter of various fractions in indoor and semi-indoor areas. The challenge is to evaluate pollution in different situations, taking into account the type of parking space and the nature of the traffic and the current air traffic conditions.

2. Materials and Methods

2.1. Ultrafine Particle Motion

The translational motion of the i-th particle under consideration is described by applying Newton's second law:

$$m_i \frac{d^2 \mathbf{x}_i}{dt^2} = \mathbf{F}_i(t) \tag{1}$$

where $\mathbf{F}_i$ is the total force acting on the i-th particle. It also evaluates contact forces; m_i and $\mathbf{x}_i$ are the mass and position of the i-th particle. Particle acceleration $\mathbf{a}_i$ is defined as

$d^2\mathbf{x_i}/dt^2$ (Equation (1)), which is the second derivative of position $\mathbf{x_i}$ vector with respect to time t.

If we define the normal orientation of contact by unit vector N, force vector $\mathbf{F^N} = F^N \mathbf{N}$ may be described by time-dependent scalar variable $F^N(t)$ [28]. The interaction of a particle in the normal direction can be described by five forces of a different nature:

$$F^N(t) = F^N_{deform}(t) + F^N_{attr}(t) + F^N_{attr\text{-}diss}(t) + F^N_{double\text{-}layer}(t) + F^N_{drag}(t) \qquad (2)$$

where $F^N_{deform}(t)$ is the particle deformation force in the normal direction (Hertz model); $F^N_{attr}(t)$—force of attraction of a particle in the normal direction; $F^N_{attr\text{-}diss}(t)$—dissipative force of a particle in the normal direction associated with adhesion [29]; $F^N_{double\text{-}layer}(t)$—electrostatic double layer force of a particle in the normal direction [30]; $F^N_{drag}(t)$—fluid drag force (Stokes model) of a particle in the normal direction. A more detailed description of the model can be found in [27–30].

Estimating the action of the normal force $F^N(t)$, the adhesive-dissipative interaction of a particle with a surface can be divided into two parts (Figure 1).
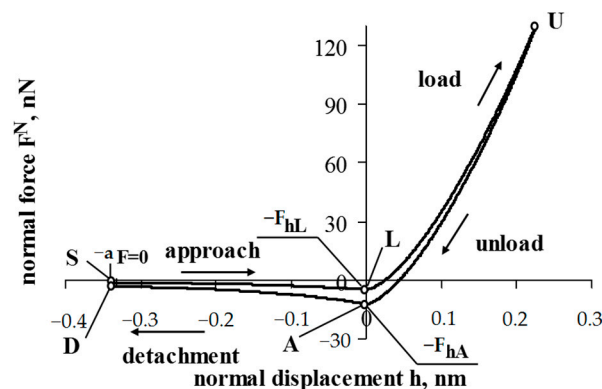

Figure 1. A model of action of dissipative-attractive forces at normal interaction. Dependence of normal force and displacement.

The first part is approach (S-L) and detachment (A-D). When approaching and detaching, the particle experiences the action of the adhesive force and, accordingly, moves at a certain distance from the interacting surface, while its displacement is considered negative. The second part includes loading (L-U) and unloading (U-A). During loading and unloading, the particle comes into contact with the surface, it is deformed, and the displacement is considered positive. In Figure 1, a negative normal force corresponds to attraction, and a positive normal force corresponds to repulsion.

All values of initial parameters for particle and epithelium cell and the references were presented in Table 1.

Table 1. The initial data.

Objects	Initial Parameters	Values	References
	Diameter, d_1	100 nm	–
	Diameter, d_2	300 nm	–
	Initial interaction distance, h_S	–	–
	Initial velocity, v_0	−1.50 m/s	[30]
	Mass, m_i	9.32×10^{-19} kg	–
Particle	Effective density, v_i	1.78 g/cm^3	[31,32], 1.2 g/cm^3)
	Young's modulus, E_i	0.14 kPa	[25]
			–
	Poisson's ratio, v_i	0.25	(Jasevičius et al., 2014, 2017)
	Surface potential, ψ_i	−39.1 mV	[26]
	The adhesion force (point L), $F_{L,adh}$	−0.6 nN	[25]

Table 1. *Cont.*

Objects	Initial Parameters	Values	References
Epithelium Cell	Density, ρ_j	1.039 g/cm^3	[32]
	Young's modulus, E_j	1.0 kPa	[33]
	Poisson ratio, ν_j	0.5	[34]
	Surface pential, $\psi_{j,I}$.	−10 mV (type I cell)	[35]
	Surface potential, $\psi_{j,II}$	−9 mV (type II cell)	[35]
Alveoli water	PH	6.9	[36]
	Temperature, T_{temp}	36.8 °C	–
	The permittivity of the free space, ε_0	8.854 × 10^{-12} C^{2}J^{-1}m^{-1}	–
	Debye length, λ	0.72 nm (physically) 0.77 nm (theoretically)	[37] [37]
	A dielectric constant of water, ε	80	[37]
	Viscosity, η_f	0.001 Pa·s	[38]
Alveoli	Diameter, $d_{alveoli}$	≈ 200 μm	

2.2. Numerical Estimation of Air Flows in a Principled Model

To determine the movement of air flow in the underground space of the parking area, a basic model 100 m long, 20 m wide, and 5 m high was developed, the scheme and calculation grid of which are shown in Figure 2.
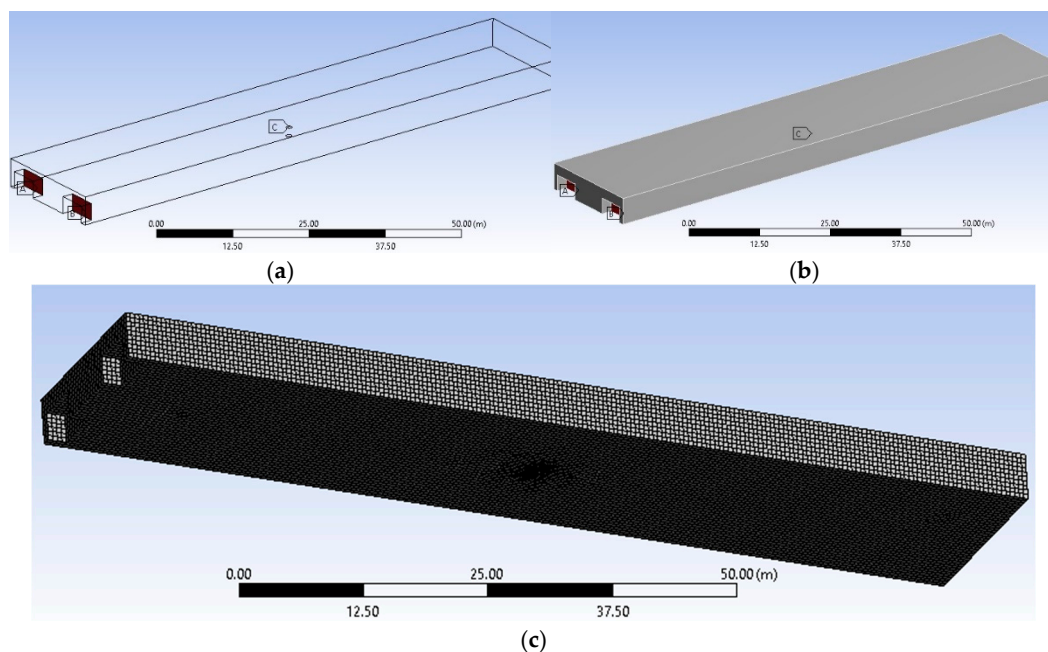

(a)

(b)

(c)

Figure 2. A principal model of the parking space for assessing the movement of air flow: (**a**) sketch and (**b**) visual model, (**c**) mesh view; A—outflow, B—inflow, C—inhalation of the respiratory system.

The design of the principal model was obtained in the CAD graphical editor program. The parameters of the model were chosen to match the standard-average of the typical parking space. The investigation and analysis of a single-phase gas flow in the device were made using the ANSYS Fluent. The computational grid was triple: in the first case, 250,125 thousand elements formed by an automatic method; in the second case, consisting of 100 thousand elements, consisting of a mixed method of Hex Dominant from Quadrum and Triangle; in the third case, 350 thousand elements compiled via the Cartesian method. In all cases, the inflation function was determined in 12 layers with a growth factor of 1.5. Initial and boundary conditions for findings the solution of principal model are: inflow (four different velocity cases), outlet (four different pressure cases). The processes in the principal parking space are constant and unchanging; oscillations in the residuals plot

were not persistent; therefore, the solution was conducted using a steady-state method. The model consists only of the main parts: the entrance gate (inflow), the exit gate (exit), and the position of the closed parking lot user in the centre of the parking lot (respiratory system). To determine the initial conditions, the velocity parameter was adopted and the cases were studied at 0.5 m/s, 1 m/s, 3 m/s, and 5 m/s. The total pressure parameter was applied to the outflow when it was 0 Pa, 5 Pa, 10 Pa, and 20 Pa. In the position of a person at a height of 1.5 m, a plane is created in the model that simulates a breathing apparatus. Studies have shown that the pressure during inspiration can reach 29–74 mm Hg [39,40]. For this, the boundary conditions in this plane are expressed in terms of static pressures equal to 29 mm Hg. Art., 45 mm Hg. Art. and 74 mm Hg. Art., which is 3.85 kPa, 6.0 kPa and 9.9 kPa, respectively.

A computational mesh consists of cells with 0.1 m long ribs for a low level, 0.05 m for average, and 0.01 m for a high level of detailing, while the elements are spaced at a distance of 0.1 m for each case. A defeature size is 0.1 m, and the curvature minimum size is 0.1 m. In the boundary zone, the mesh has a maximum of twelve layers. The growth rate is 1.5. The value of the y+ in the first cell next to the solid boundary was 0.36 for all three meshes. It was used as a standard solution initialization.

2.3. Field Research

For experimental studies, several closed and semi-closed underground parking lots were selected. Each of the surveyed sites (parking lots) differs in the location, number, and size of vehicles in the trajectory of cars, light trucks, and trucks in the area, traffic flows and occupied area, entrance/exit from the outside and exit/exit from the parking lot to the outside. Studies in each individual parking zone were carried out in the winter and spring seasons of 2021–2022, and environmental parameters were assessed in different cold and warm seasons and their possible impact on pollution in the studied areas.

Air pollution studies of fine particulate matter were conducted using a Fluke 985 numerical particle counter. Particle concentrations were determined in each study in six size ranges: less than 0.3 μm, 0.5 μm, 1.0 μm, 2.0 μm, 5.0 μm, and 10.0 μm. The sampling rate is 0.1 cfm (2.83 L/min). Device counting efficiency is 50% for 0.3 μm size and 100% for >0.45 μm size particles. Zero count level is equal to 1 count/5 min. A two-pronged approach to data collection was used, depending on the sample volume or draw time. The results were repeated until there was a repeatability and a difference between the minimum/maximum of no more than 5%. In each zone, at separate points, research was carried out under the same meteorological conditions, placing the measuring equipment at significant points according to the diagrams in Figure 3. The determination of concentration was based on a class 3B laser source with a wavelength of 775–795 nm and a power of 90 mW. The efficiency of calculations based on ISO 21501, i.e., a 50% probability for particles with a size of 0.3 μm are determined with a 100% probability for more than 0.45 μm.

To calculate the mass concentration (C) in kg/m^3 of particulate matter, a conversion of the numerical concentration of particles was used in accordance with Equation (3):

$$C = N \cdot \rho \cdot \frac{4}{3} \cdot \pi \cdot R^3 \tag{3}$$

where N is the number of aerosol particles of a given size in m^3 of air volume; by default this volume is equal to 1 m^3, ρ is the particle density in kg/m^3, the standard density of indoor particles is assumed to be 1800 kg/m^3, R is the particle radius, m, for each case this radius in μm is equal to 0.3, 0.5, 1.0, 2.0, 5.0, and 10.0.
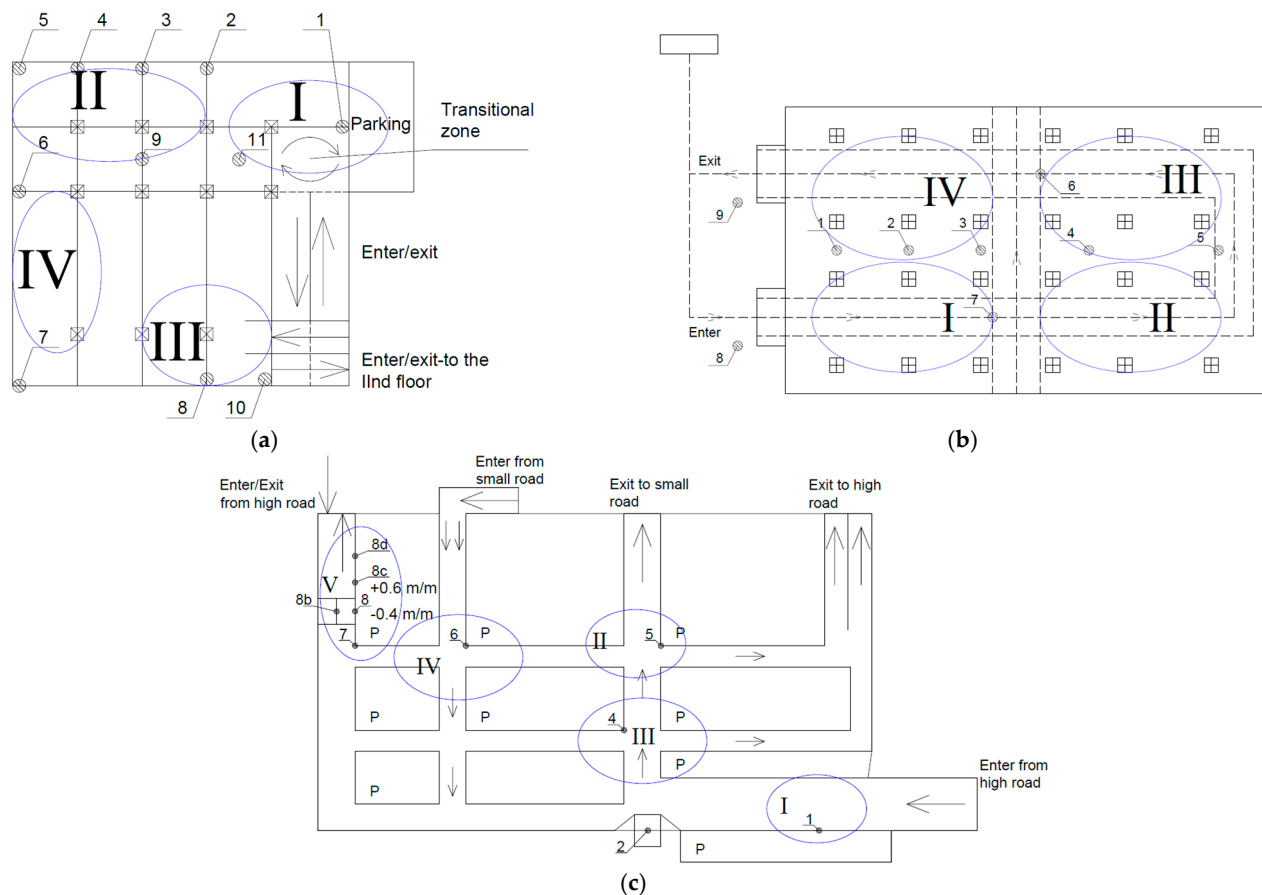
(a)

(b)

(c)

Figure 3. A principal view of the closed area and the air pollution research site (**a–c**).

The purpose of the experimental studies was to determine the present amount of fine and very fine particulate matter in the ambient air of various types of indoor areas. The main purpose of this part of the study is to analyse the levels of pollution in the area of each zone and determine the conditions for maximum pollution. The numerical concentrations of particles were studied at different heights of 0.1 m, 1.0, and 1.5 m at ground level, the lumbar area, and relative to the human inhalation zone. During each study, the number of passing vehicles, the direction of their movement, and other circumstances were recorded. Both instantaneous and short-term air pollution in the immediate vicinity of the vehicle (cars) as a source of pollution has been identified. To assess the level of pollution at different sites, a sampling time of at least 60 s was taken, and the same number of passing vehicles was used. Schemes and points of study of various closed parking areas are shown in Figure 3.

Zone A: area 700 m^2, volume 2800 m^3. The territory is installed on raised foundations, and on three sides the site is completely insulated with walls, while on the one hand there is an entrance/exit for the site and windows installed at a height of 1 m and at a height of 1.5 m. Movement on the territory occurs in a circle in one lane; parking areas are installed throughout the periphery and in the center of the area. Zone B: area 1500 m^2, volume 6750 m^3. The territory is located on the ground floor, the site is fully insulated from all sides, and there is a separate gate for entry/exit. Traffic in the area is in one direction, while in two lanes, parking areas are installed along the entire periphery and on an intermediate platform in the centre. Zone C: area 6800 m^2, volume 17,000 m^3. The parking area is located on the ground floor, the area is fully insulated from all sides, and the entrance/exit is equipped with ordinary and tunnel-type passages.

Traffic in the parking lot occurs in sections. In one section, there is movement in two directions in one direction, while in the neighbouring section, there is movement in the opposite direction along two lanes. In total, there are three entrances to the parking area;

the traffic on them is one- or two-lane. In total, there are three exits from the parking lot: where the traffic is single-lane and at the exit from the tunnel, there are two lanes with one-way traffic. Parking spaces are provided in each section.

3. Results

3.1. Field Research

The results are presented in Figures 4 and 5. The S-L-U-A′ points describing the interaction are evaluated, the values at these points are presented with a change in force, and velocity and displacement are given in Table 2. At the same time, the description of these points is given in Figure 1.
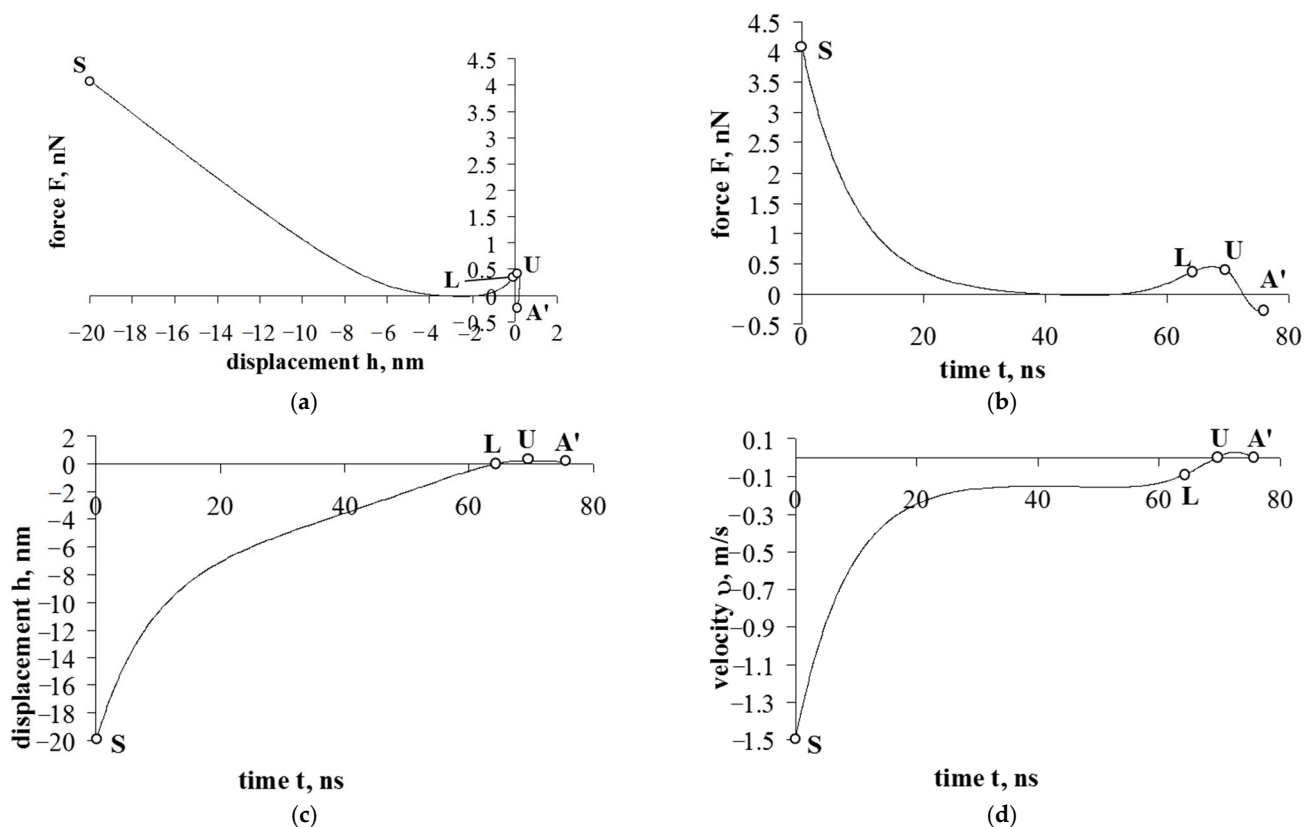

Figure 4. Particle interaction in alveolus. Particle diameter: 300 nm. (**a**) normal force F versus displacement h; (**b**–**d**) history of normal force F, displacement h, velocity υ, respectively.

Table 2. Particle interaction properties during interaction at certain points S-L-U-A′.

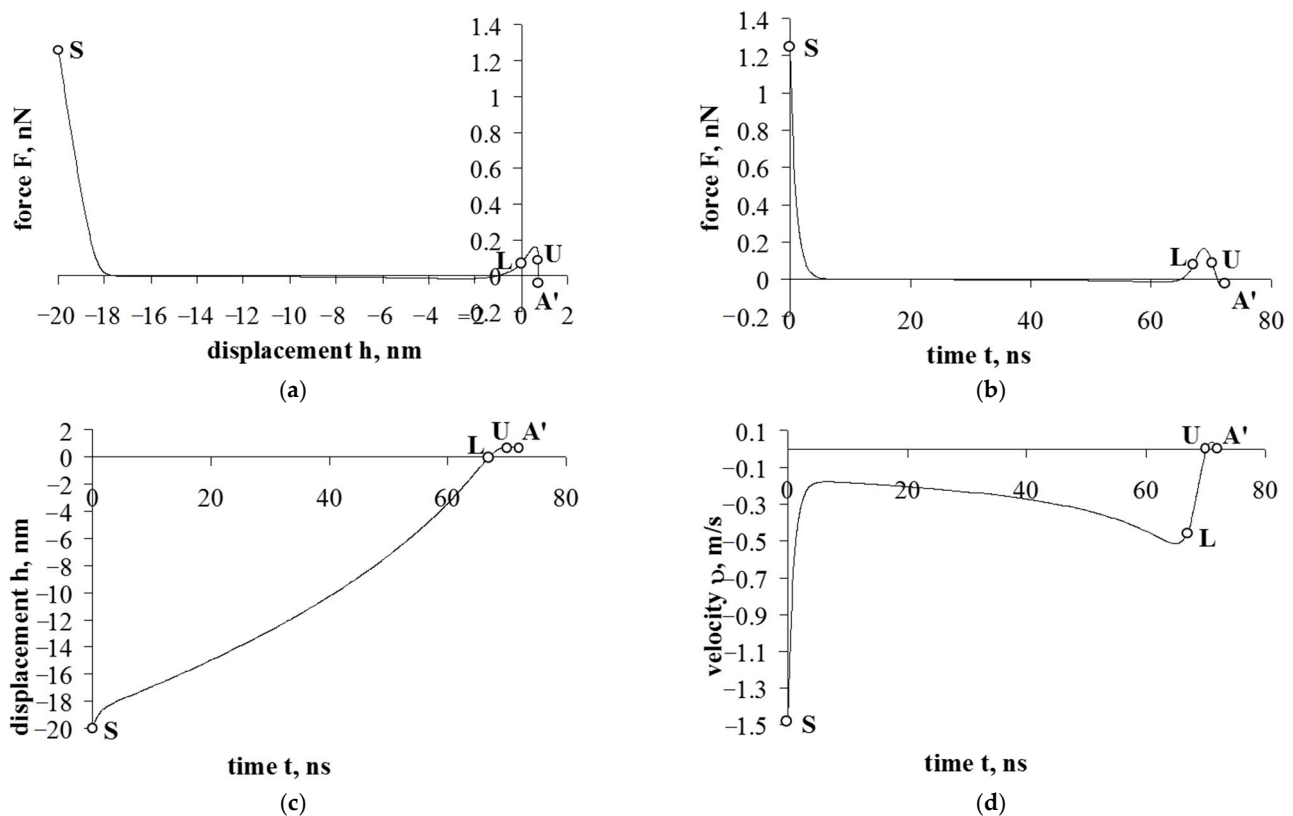| Diameter Parameter		Values at Certain Points			
		S	**L**	**U**	**A′**
100 nm	t, ns	0	66.985	70.198	72.231
	F, nN	1.264	0.06914	0.0845	−0.03
	h, nm	20	0	0.750	0.703
	v, m/s	−1.5	−0.4536	0	0
300 nm	t, ns	0	64.401	69.583	75.847
	F, nN	4.091	0.375	0.4	−0.279
	h, nm	20	0	0.232	0.126
	v, m/s	−1.5	−0.08841	0	0

Figure 5. Particle interaction in alveolus. Particle diameter: 100 nm. (**a**) normal force F versus displacement h; (**b–d**) history of normal force F, displacement h, velocity υ, respectively.

3.2. Numerical Modeling of Air Flows

The laminar flow viscosity model was chosen, using the solution which converged, and residuals of 10^{-5} order were achieved. A numerical model was developed to find representative areas and predict study points based on existing airflow paths where the results would reflect the total concentration of particulate matter generated, as well as specific locations requiring additional evaluation. The distribution of airflow velocity was in a principally enclosed space with inlet and outlet and a potential person in the centre during inhalation. Several cases were considered, and the results are obtained in Figure 6, when the inflow speed (wind speed) at inflow was: 0.5 m/s, 1 m/s, 2 m/s, 3 m/s, 4 m/s, and 5 m/s.

The model results showed that at low inflow velocities (0.5–2 m/s), the air paths only partially reach the central zone, so it is necessary to analyse points on both sides of the sites, and concentrations cannot be considered to be symmetrically distributed throughout the closed zone. The simulation results also showed that the flow from the inflow deviates more towards the outflow than into the closed area when the speed reaches more than 4 m/s. It is also noted that air vortices are formed near the inflow and outflow; therefore, in field conditions, it is necessary to select points for research at least 3–5 m from the "gate" of air inflow. To refine the situation, the model analysed the case when the inflow velocity is likely to be about 1 m/s. The distribution of air flow in different sections and in a vertical section is shown with the position of the closed parking lot user in the centre of the space (inhaled by the air of the respiratory organs) (Figure 7).
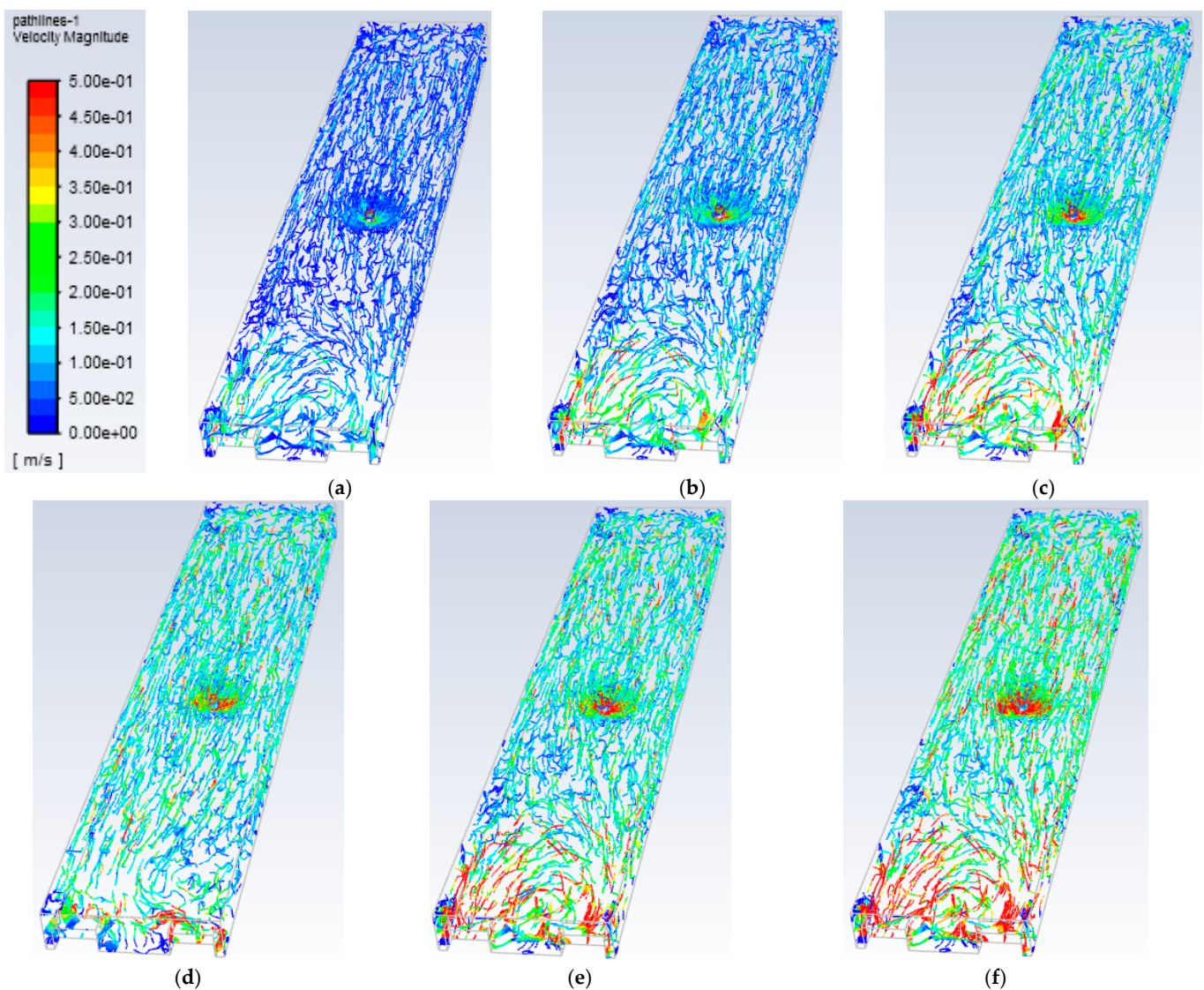
Figure 6. Distributions of air flow at different inflow velocities: (**a**) 0.5 m/s, (**b**) 1 m/s, (**c**) 2 m/s, (**d**) 3 m/s, (**e**) 4 m/s, (**f**) 5 m/s.

The model confirms the previously observed phenomenon when, at an air inflow velocity of 1 m/s, the air flow is higher than 0.3–0.4 m/s only in the central part of the first side of the object. Later, in the centre, there is a mixture of flows over the entire section due to the influence of the respiratory organs on the situation. When moving away from the inflow on the other side of the model object, the air flow only closer to the wall exceeds the minimum values and does not exceed 0.2 m/s. As shown in Figure 7b,c which differ only in reference scale, the air flow paths extend from the entire space towards the closed parking lot user and reach up to 15 m/s at the air intake itself. Airflow velocities in space vary from 0.4 to 1.6 m/s around the position of a closed parking lot user.

To describe the air flow in the model space, various display methods were chosen, which are shown in Figure 8. In essence, three main zones 1, 2, and 3 are formed in the entire space—near, central, and far, respectively. Each of them forms its own vortices, the trajectories of which extend to the adjacent neighbouring zone, and thus the flows are mixed throughout the entire zone, which transports solid particles and distributes them throughout the volume. At the same time, at a low inflow rate (1 m/s), only the central part created higher inspiratory flows, reaching 1–1.6 m/s. In section No. 3 (Figure 8), there is also a "blind" zone (Figure 8, area 4), through which flows flow and do not enter.
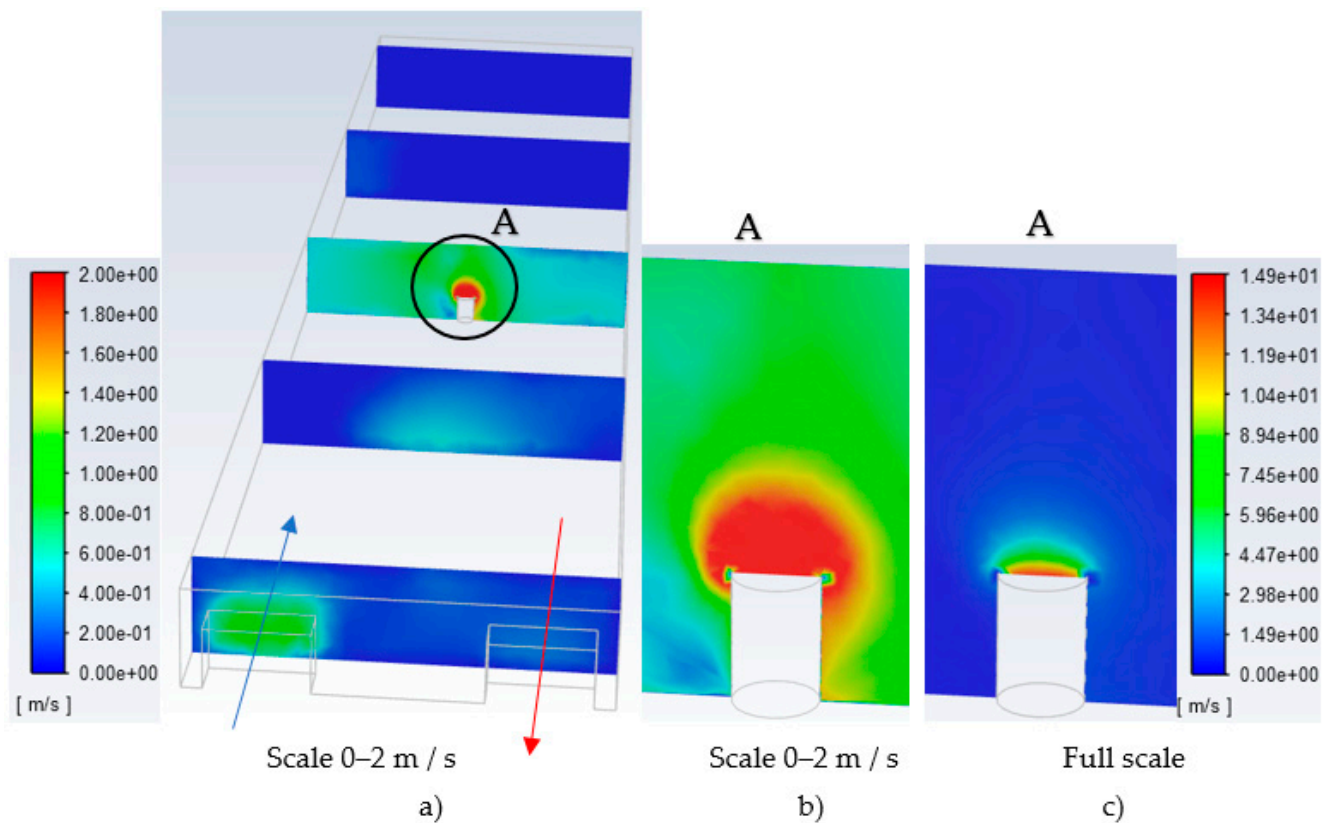
Figure 7. The distribution of air flow velocity: (**a**) by sections; (**b,c**) at the location of the closed parking lot user (human) in the centre of the space (inhaled air of the respiratory system) in scale 0–2 m/s and in full scale.

Figure 8. The distribution of air flows from inflow to potential human airways and outflow, scaled to 0–2 m/s.

One of the biggest influences on air flow and particulate transport is the flow turbulence, which is defined by Reynolds numbers. Compared to air flow, the migration of fine particulate matter is much more complex due to its high density, so it can be assumed that

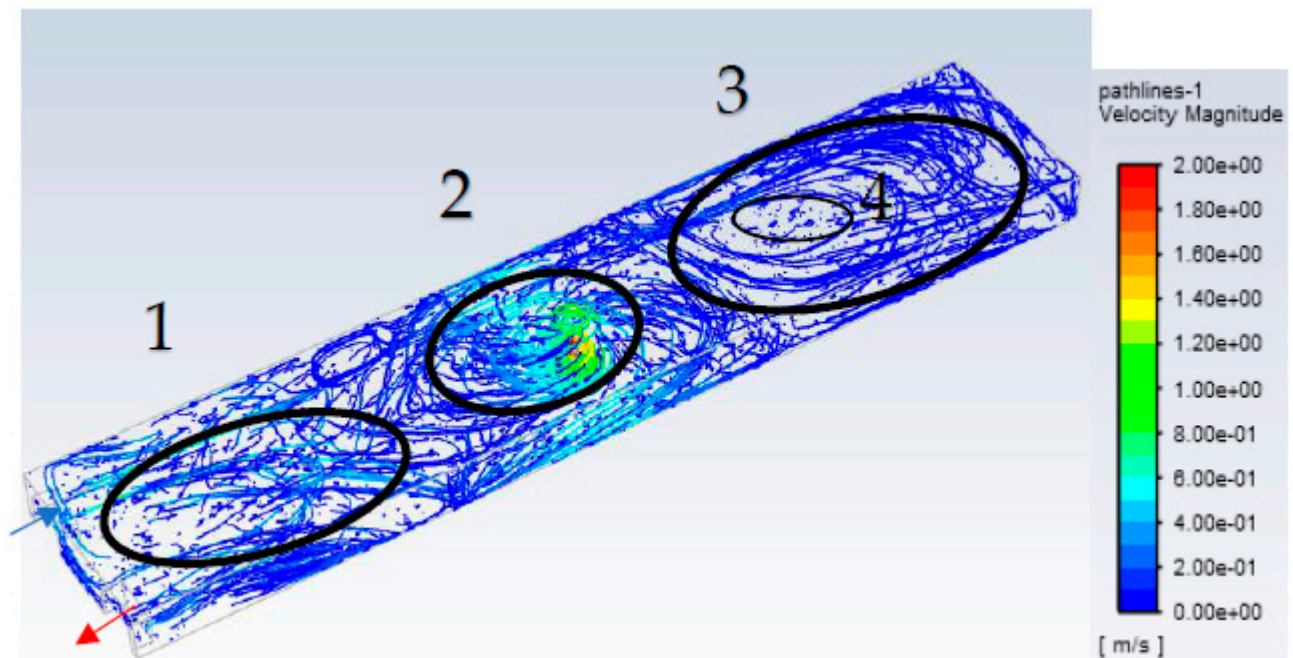laminar and indeterminate flow motion can carry only a part of the smallest fraction of particles (0.3–1 μm in size).

The object of the numerical model is divided into segments by position, and each of them represents the distribution of the Reynolds number (Figure 9). According to the results, the largest particle transport is likely to occur in the central zone. Reynolds numbers above 5×10^4 were also found in adjacent zones, with a more uniform decrease observed in the rear zone. However, slightly less than half of the Reynolds number points in the overall model space have indeterminate motion and only a few are laminar at the edges of the closed zone.
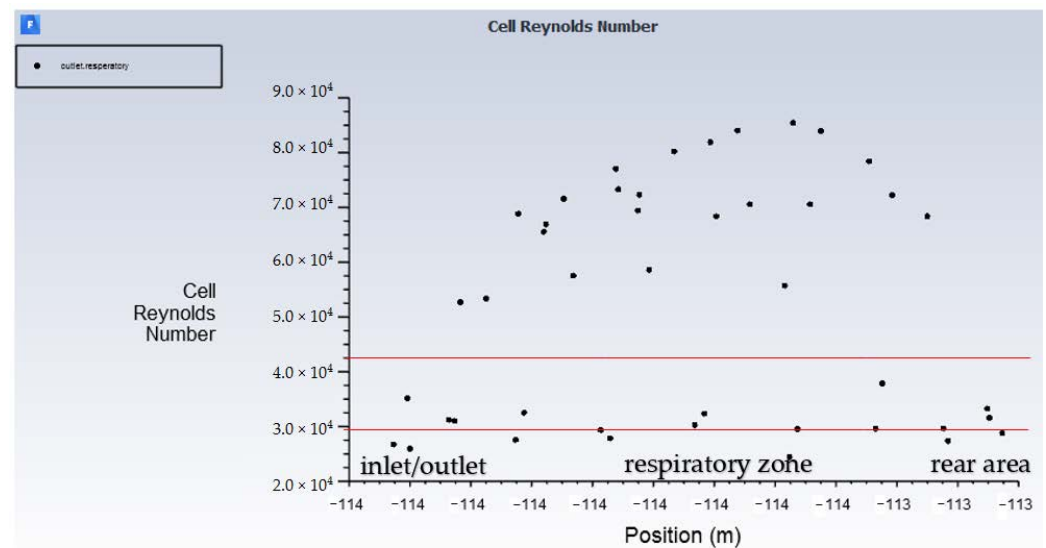

Figure 9. Variation of the Reynolds number in the longitudinal section of the object.

The results obtained in the course of field experimental studies represent the actual pollution generated by ultrafine and fine particulate matter in various types of enclosed spaces, taking into account various microclimatic conditions and circumstances and places of occurrence of pollution. In the first stage, the parameters of microclimate conditions, which are presented in Table 3, were investigated.

Table 3. Microclimate parameters in enclosed spaces.

Parameter	Parameter Values at a Eight of 0.1 m/at a Height of 1.0 m/at a Height of 1.5 m		
	Temperature, °C	Relative Humidity, %	Air flow Rate, m/s
At the entrance:			
Zone A	2.1/2.8/3.1	71.1/70.5/69.9	0.31/0.37/0.45
Zone B	2.9/3.5/3.9	65.5/64.6/63.1	0.21/0.27/0.31
Zone C	2.3/2.5/2.8	66.3/65.9/65.7	0.25/0.28/0.32
At the exit:			
Zone A	2.5/3.0/3.4	71.1/70.5/69.9	0.32/0.38/0.43
Zone B	3.1/3.7/4.0	65.5/64.6/63.1	0.23/0.29/0.32
Zone C	2.5/2.8/3.1	66.3/65.9/65.7	0.27/0.29/0.33
Across the inner space:			
Zone A			
I	3.4/3.7/4.1	60.5/59.6/59.1	0.21/0.27/0.31
II	3.7/3.9/4.2	58.3/57.1/56.8	0.22/0.26/0.32
III	3.5/3.8/4.1	58.5/57.5/57.9	0.23/0.26/0.29
IV	3.7/3.8/4.0	58.2/57.3/57.7	0.22/0.25/0.30
Mean	3.6/3.8/4.1	58.9/57.9/57.9	0.22/0.26/0.31
Standard Deviation	0.1/0.1/0.1	0.9/1.0/0.8	0.01/0.01/0.01
Zone B			
Mean	3.9/4.1/4.5	57.2/56.2/56.2	0.23/0.27/0.32
Standard Deviation	0.1/0.1/0.1	0.9/1.0/0.8	0.01/0.01/0.01
Zone C			
Mean	3.8/4.1/4.4	55.4/54.5/54.5	0.23/0.27/0.31
Standard Deviation	0.1/0.1/0.1	0.9/0.9/0.8	0.01/0.01/0.01

Table 3. *Cont.*

| Parameter | Parameter Values at a Eight of 0.1 m/at a Height of 1.0 m/at a Height of 1.5 m | | |
	Temperature, °C	Relative Humidity, %	Air flow Rate, m/s
Outdoor conditions at:			
Zone A	0.7	85.3	3.1
Zone B	1.2	72.3	3.8
Zone C	1.0	69.6	4.2

The detailed results of the assessed conditions of the individual zones of the microclimate showed the essential trends at each level and the even distribution, which can be deduced from the standard deviation values, and which is important for the assessment of particulate pollution. A more detailed analysis of the results for zone A revealed that the values of the parameter of relative humidity changed the most. The air flow velocity is increasing in terms of results at a height of 0.1–0.22 m/s to 0.31 m/s at a height of 1.5 m. In other zones, the air temperature was not higher than 0.8 °C compared to all altitudes, the lowest relative humidity zone is C, and the overall average is 54.8%; the maximum air flow rate is set in zone B at a height of 1.5 m and is equal to 0.32 m/s. Field meteorological conditions during the measurements are presented in Table 3.

Numerical concentrations of particulate matter were measured in all three zones, and the values of different particle fractions and their change at individual points of the zones are given. The results of the tests in zone A are given in Table 4. The values obtained show that low concentrations of all fractions were obtained at points 5–8, which are located in the parts of zones II–III–IV A, which are remote from the place of entry, but there was no more than 1 measure of passing cars. High concentrations of ultrafine particles are found in Item No. 2, which is located in the intermediate zone between Parts I and II, and had a mass concentration of 1.05 µg/m^3 in the fraction of particulate matter greater than 0.3 µm, 3 vehicles passed during the test period. The maximum concentration of 2 µm was determined at point No. 3, which reached 0.015 µg/m^3 recorded at this point, and the average concentration of ultrafine particles 0.3–5 µm, for example, 5 µm, was 90 units.

Table 4. The mean numerical concentrations of particulate matter at a height of 1.5 m in zone A.

| Test Point No. | Numerical Concentration of Particles Not Smaller than the Specified Size (µm), Units | | | | | | Average Number of Cars |
	0.3	0.5	1	2	5	10	
1	34,365	6453	2565	630	53	7	2
2	58,658	8452	2994	731	66	5	3
3	36,163	7628	3147	847	90	6	1
4	43,474	7613	3169	812	94	8	1
5	53,597	7785	2851	691	72	5	1
6	39,613	6862	2670	660	71	5	1
7	47,043	7578	2928	741	68	3	0
8	44,371	7099	2737	688	69	4	2
9	66,498	8006	3162	828	102	8	2
10	45,894	7393	2789	675	81	6	2
11	38,136	6941	2775	699	89	7	2

Assessing all parts of the study of zone A, it can be stated that it was dominated by medium concentrations of fine particulate matter of 1–10 µm, and high concentrations of 0.3–0.5 µm and 2–10 µm. The maximum concentrations of 1 µm of particulate matter are found in Part II at points close to the angle, which is the remote part of the site affected by both the air currents lifting the larger particles and the passing 2 vehicles. For large fine

dispersion particles with a size of 5 to 10 μm set at points 10 and 11, this indicates that the parts of the site at higher inlet/outlet flows, which lift the largest particulate matter, were also affected by the passage of 2 vehicles.

In zone B, the geometry is symmetrical, provided that the entrance and exit are arranged on the same side. Concentrations in this zone are more than twice as high, and there is a greater dispersion between the test points and the numerical concentrations of the particulate fractions analysed (Table 5). Low concentrations of all fractions were found at points in Part IV (points 1 and 2) where there were no passing vehicles. Irrespective of the number of vehicles passing, high concentrations of ultra-fine particles were found at points 3, 4, and 6, and in this case point 3 recorded the highest concentration in the whole area—over 116 thousand particles, which corresponds to 2.1 μg/m^3 concentration where no vehicles were detected. The numerical concentrations of the particles in the middle fraction (1, 2, and 5 μm sizes) were highest at point numbers 2079, 665, and 125 particles, respectively.

Table 5. Mean numerical concentrations of particulate matter at a height of 1.5 m in zone B.

Test Point No.	Numerical Concentration of Particles not Smaller than the Specified Size (μm), Units						Average Number of Cars
	0.3	0.5	1	2	5	10	
1	86,775	6164	1677	497	87	1	0
2	87,495	6358	1658	493	82	1	0
3	116,438	8023	1989	538	69	2	0
4	110,691	7579	1890	555	91	3	0
5	97,392	7416	2079	665	125	7	1
6	105,723	7479	1988	639	114	6	0
7	96,512	7038	1977	613	112	2	0
8	104,724	6630	1737	593	123	11	0
9	96,286	6966	2003	662	124	9	0

Analysing the distribution of the average concentration of fine particulate matter 1–10 μm, it can be stated that the average concentrations in the centre of zone B are maintained; for example, at point 6 the particles reach 0.5 μm—7479 units and 5 μm—114 units. At some points in the area close to the point of entry and exit (points 7 and 9), high concentrations of particulate matter between 1 and 5 μm were detected, and at point 8 the largest was 10 μm, although no vehicles were present. This trend is repeated in Zone A and can be said to be significantly influenced by the elevated pollution at the site itself, which is made up of larger fractions of particles, and the increase in such pollution is most noticeable at the margins or near the entrance/exit gates for larger particles, i.e., 5 and 10 μm at Point 8.

In Zone C, it was possible to investigate situations that often occur in confined spaces with traffic. For example, at point 2, the study was carried out between two lanes in the same direction; the wind speed in this space is 1.5–2.5 m/s and the concentration at this point was average compared to the whole zone C—0.3 μm of particles were found above 51 thousand, which corresponds to 0.93 μg/m^3 (Table 6). At point 8, pollution from the conditions of the complex was analysed—a point between the rows in a different direction, and the road with an ascent of 0.6 m/m leading towards the exit.

Table 6. Mean numerical concentrations of particulate matter at a height of 1.5 m in zone C.

Test Point No.	Numerical Concentration of Particles Not Smaller than the Specified Size (μm), Units						Average Number of Cars
	0.3	0.5	1	2	5	10	
1	37,135	4041	1120	244	35	3	2
2	51,641	5493	1561	326	47	3	4
4	59,913	6550	1814	361	44	2	3
5	63,969	6509	1768	327	38	2	3
6	122,635	15,580	3906	642	63	3	1
7	109,927	13,059	3342	562	53	3	4
8	49,799	5240	1508	326	46	5	3
Before lifting	39,425	4480	1308	286	38	4	3
Lifting	42,667	4953	1177	259	35	4	3
End of lifting	52,026	5075	1171	258	43	6	3

The highest concentrations were found at entry point 6, where they reached 2.2 μg/m³ concentrations. At the exit at the parallel level at point 7, and a concentration close to 1.97 μg/m³ was detected. In both cases, the particulate values of all fractions are highest in this zone except for 10 μm. In the part of the site where the road is equipped with a slope, only slightly higher concentrations of fine particles ranging from 0.71–0.9 μg/m³ and an increase in the largest 10 μm with numerical concentrations of 4 to 6 units were found, while in other cases there were no more than 3 units.

4. Discussion

From the perspective of air circulation in parking lots, the aim of these studies was to investigate one of the most common enclosed spaces, such as car parks, where pollution is often favourable and the person entering the area is forced to inhale airborne pollutants.

The velocity of the inhaled air flow at the closed parking lot user is approximately 1.6 m/s, and this is sufficient to transport pollutant particles from the close environment of the closed parking lot user, in this case, from the motor vehicle as a source of pollution. If the velocity of movement is caused by the air ventilation system or through the entry/exit gates, the probability of entering to the "breathing zone" at the center part of the parking lot only increases. Characteristic zones were determined for the numerical model of the main object, and the movement of the air flow in a closed space with a potential human respiratory system in this zone was determined. Field studies of particulate matter concentrations were carried out at representative locations to assess traffic flows, and the microclimatic conditions of each of the three enclosed spaces were analyzed.

First, it was important to examine the entry of particles into the lungs, the alveoli. As it approaches the alveolar wall, the particle is subjected to an overall force, including alveolar fluid effects and adhesion. The extremely small nanoparticle is supposed to move with the airflow until it reaches the alveolus, the alveolar fluid on its surface.

It is assumed that at the initial time, the particle is already in the alveolar fluid. Since the direction of motion of the particle is perpendicular to the surface of the alveolar cell, it is assumed that the particle moves only in the normal direction, and its motion in the tangential direction is not considered. Let us first discuss the action of the normal force on the particle. The results are presented in Figures 4 and 5.

When the particle approaches the surface of the alveolar wall, their interaction is reflected in this study by points (S-L). The results show that when interacting in a liquid, when a particle approaches, at the beginning of the interaction, the repulsion force is quite large. Later, as the interaction continues and the particle approaches the surface, the thrust force decays, but increases again when the particle almost approaches the interacting

surface and the contact. During contact, the repulsion force increases a little more (L-U) and unloading begins (U-A′). The repulsion force achieved at the contact is much less than at the beginning of the interaction. When the particle reaches point (A′) during unloading, the reload starts. The further movement of the particle under reload is considered as a sticking process, which is not considered in this paper. A description of the particle sticking process can be found [27]. In the process of sticking, the motion of the particle stops when the value of the total force remains equal to 0.

Let us now discuss the change in the velocity of particles upon interaction. The particle velocity decays during approach (S-L) and then stabilizes. When the particles come into contact, the velocity decay increases again (L-U), the velocity direction changes (U-A′), and after reaching point A′, the velocity is 0. As mentioned earlier, when point A′ is reached, a sticking process follows, which is not considered in this paper. In the process of sticking, the motion of the particle stops when the value of the velocity remains equal to 0.

Finally, let us discuss the change in particle displacement during interaction. The displacement of the particle upon contact is much less than the distance of the particle at the beginning of the interaction. It should be noted that at the beginning of the interaction, the distance between the particle and the alveolar cell is 20 nm; it is assumed that at this distance, the particle is affected by the forces of adhesion and the electrostatic double layer. When the particle reaches point A′ on contact, a reload will occur, which is considered the beginning of the sticking process. As already mentioned, the sticking process is not considered further, but it is indicated that when a particle sticks, it will stop with a residual displacement h. Also, as already mentioned, due to the extremely short duration of interaction, the alveolar wall is considered stationary. If, after estimating a significantly longer time than that considered here, the displacement and position of the adherent particle can change as the person fully inhales and exhales.

The cases shown in Figures 4 and 5 reflect the expected behaviour of particles (diameter values of 100 nm and 300 nm, respectively) when an inhaled nanoparticle reaches the alveolar surface. Although the behaviour of force, velocity, and displacement of the two previously discussed diameters is the same, it is also important to discuss the differences in interaction. When studying a smaller (100 nm) particle, the obtained force values were lower, but the particle had a higher approach velocity (S-L) and a larger displacement value was achieved at point A′. The results show that the particle, although subject to the resistance of the alveolar fluid, easily reaches and interacts with the surface of the cell, forming the alveolar wall in a particularly short time.

Given that the alveolus pulsates when breathing, this will also affect the interaction. Since in this case the interaction lasted for nanoseconds, it is many times shorter than it would be required for a person to take a full breath. It is important to note that, therefore, when simulating the interaction of a particle in the alveolus, the inner surface of the alveolus remains stationary as the particle moves towards the alveolar wall.

In the performed studies, the arrangement of field measurement points according to the prevailing flow trajectories in the numerical model was selected (Figure 6). Studies of fine particulate matter have shown that indoor pollution is potentially harmful to the person inside. The respiratory system, especially with low air movement in space, receives a dose of pollutants from the air from almost half the volume of space when the area is about 10 thousand m^3. At a flow rate of 1 m/s, the space is dominated by air flows with a Reynolds number in the range of 3–8 $\times$ 10^4 (Figure 7).

In the three closed spaces presented in Table 3 selected by field research the parking lots of motor vehicles, the microclimate parameters confirmed that the temperature and relative humidity changed insignificantly, and the air flow speed was about 0.22–0.32 m/s. The maximum interval between values is set at entry and exit. The speed at 1.5 m (height) was more than 1.15 and 1.3 times higher than at 1 m and 0.1 m, respectively. Particulate matter has been found to accumulate in blind spots in enclosed spaces and in the centre of sites where concentrations of more than 1 μg/m^3 are observed in a relatively small number of vehicles. It has been studied that 0.5 μm of particles are reduced by almost 10 times and

1 μm by about 25 times compared to 3 μm of particles. Larger particles are found in almost all cases along the edge walls of the closed area, and at the entrance/exit gate. The terrain of the site has a particularly significant impact on air pollution in such locations. Particularly high and more than 2–3 times higher concentrations were found in the lower zones at the abrupt entry/exit. Significantly more fine particles of 0.3–0.5 μm are detected in these areas. Concentrations ranging in size from 1 to 5 μm are up to 0.07 μg/m^3 (Tables 4–6).

5. Conclusions

Regarding the entry of particles into the lungs via the human respiratory tract, an additional task and extension of this study was to study pollution by fine fractions of particulate matter, which, when inhaled with air, can enter the deep tissues of the respiratory system and accumulate in organs. The results show that inhaled diesel particles can reach the alveolar wall. In addition, when comparing the interaction of 300 nm and 100 nm particles with the alveolar wall, a smaller particle can penetrate the alveolar wall much more easily, and more than a 5-fold increase in displacement (at point A′) was observed during the interaction. Surveys of different sites allow us to predict possible differences and the specifics of each enclosed space. In this case, average values or their change over time will not provide useful information about human exposure. Studies have identified short-term, momentary pollution that can affect a person after spending some time in the enclosed spaces analyzed in this study.

The results show that the air flow of diesel cars in closed parking lots affects human health; therefore, in order to improve the infrastructure of car parking, issues related to air purification should be provided/solved when designing a building. As an example, the additional installation of air cleaning devices (such as a cyclone) could be appreciated, since today's parking lots are designed to accommodate more and more cars, but as the number of cars increases, it becomes more difficult to ensure air quality. The placement of air cleaning devices should be concentrated in places with a greater concentration of cars, where it is impossible to provide sufficient circulation of clean air. Experimental results showed that it is relevant to apply air supply/suction systems in areas of high maneuverability, i.e., at turns, at intersections, and filters must be adapted to retain particles of 1–5 μm in size with a concentration of over 2 μg/m^3. On the other hand, preventive protection measures can be applied, e.g., footpaths at the mentioned "increased pollution" zones are not recommended; instead of them, the installation outside of the parking area are more effective. The results showed that when the intensity of the traffic flow is doubled, the concentration of 0.3–0.5 μm particles increases by about 20–30%, and also by about 10%, on average, of particles smaller than 2 μm. In this way, it is advisable to limit the transit of passing vehicles, which in turn additionally cause elevated pollution. Of course, one should also pay attention to the fact that recent trends show an increase in the number of electric vehicles, which in the future will lead to a natural decrease in the level of car pollution. This study helped to find out the main characteristics of closed car parking areas, the level of pollution with fine, ultrafine, and nano-sized particles. The subsequent study will allow a deeper study of the specific movement of particles depending on their size, as well as the influence of engineering equipment on a possible decrease in concentration in or around the zone of a closed parking lot user.

Further research could examine the movement of polluted air not only indoors, but also outdoors; for example, when a person moves near a busy street. Although studies have shown that pollutant particles easily interact with the alveoli of the lungs and additional indoor air purification devices are still needed, the problem of effectively reducing human exposure to pollutants remains. Therefore, further studies may also additionally include modeling the entry of air pollutants through masks that protect the human respiratory tract. Previous studies have focused on cyclone air-cleaning devices, which will continue to be researched. Numerical studies are currently underway on the possibility of using environmentally friendly filters. Therefore, this problem of atmospheric air pollution

requires many different studies, and we hope that this and subsequent studies will bring cognitive benefits to the reader.

Author Contributions: Conceptualization, A.C. and R.J.; methodology, A.C. and R.J.; software, A.C. and R.J.; validation, A.C. and R.J.; formal analysis, A.C. and R.J.; investigation, A.C. and R.J.; resources, A.C. and R.J.; data curation, A.C. and R.J.; writing—original draft preparation, A.C. and R.J.; writing—review and editing, A.C. and R.J.; visualization, A.C. and R.J.; supervision, R.J.; project administration, A.C. All authors have read and agreed to the published version of the manuscript.

Institutional Review Board Statement: Not applicable.

Informed Consent Statement: Not applicable.

Data Availability Statement: Not applicable.

Conflicts of Interest: The authors declare no conflict of interest.

References

1. Tomas, J. Adhesion of Ultrafine Particles—A Micromechanical Approach. *Chem. Eng. Sci.* **2007**, *62*, 1997–2010. [CrossRef]
2. Morawska, L.; Buonanno, G. The Physics of Particle Formation and Deposition during Breathing. *Nat. Rev. Phys.* **2021**, *3*, 300–301. [CrossRef] [PubMed]
3. Steiner, S.; Bisig, C.; Petri-Fink, A.; Rothen-Rutishauser, B. Diesel Exhaust: Current Knowledge of Adverse Effects and Underlying Cellular Mechanisms. *Arch. Toxicol.* **2016**, *90*, 1541–1553. [CrossRef] [PubMed]
4. Oberdörster, G.; Oberdörster, E.; Oberdörster, J. NANOTOXICOLOGY: An Emerging Discipline Evolving from Studies of Ultrafine Particles. *Environ. Health Perspect.* **2005**, *113*, 823–839. [CrossRef]
5. Patton, J.S.; Byron, P.R. Inhaling Medicines: Delivering Drugs to the Body through the Lungs. *Nat. Rev. Drug Discov.* **2007**, *6*, 67–74. [CrossRef]
6. ECOpoint Inc. What Are Diesel Emissions. Exhaust Particulate Matter. Available online: https://dieselnet.com/tech/dpm_size.php (accessed on 25 July 2022).
7. Abdul-Khalek, I.; Kittelson, D.; Brear, F. The Influence of Dilution Conditions on Diesel Exhaust Particle Size Distribution Measurements. In Proceedings of the International Congress & Exposition, Detroit, MI, USA, 1–4 March 1999; SAE International: Warrendale, PA, USA, 1999.
8. Kittelson, D.B. Engines and Nanoparticles: A Review. *J. Aerosol Sci.* **1998**, *29*, 575–588. [CrossRef]
9. Barone, T.L.; Lall, A.A.; Storey, J.M.E.; Mulholland, G.W.; Prikhodko, V.Y.; Frankland, J.H.; Parks, J.E.; Zachariah, M.R. Size-Resolved Density Measurements of Particle Emissions from an Advanced Combustion Diesel Engine: Effect of Aggregate Morphology. *Energy Fuels* **2011**, *25*, 1978–1988. [CrossRef]
10. De Filippo, A.; Maricq, M.M. Diesel Nucleation Mode Particles: Semivolatile or Solid? *Environ. Sci. Technol.* **2008**, *42*, 7957–7962. [CrossRef]
11. Höglund, P.G. Parking, Energy Consumption and Air Pollution. *Sci. Total Environ.* **2004**, *334–335*, 39–45. [CrossRef]
12. Kim, S.R.; Dominici, F.; Buckley, T.J. Concentrations of Vehicle-Related Air Pollutants in an Urban Parking Garage. *Environ. Res.* **2007**, *105*, 291–299. [CrossRef]
13. Vuković, G.; Aničić Urošević, M.; Razumenić, I.; Kuzmanoski, M.; Pergal, M.; Škrivanj, S.; Popović, A. Air Quality in Urban Parking Garages (PM10, Major and Trace Elements, PAHs): Instrumental Measurements vs. Active Moss Biomonitoring. *Atmos. Environ.* **2014**, *85*, 31–40. [CrossRef]
14. Takacs, A.; Haidegger, T. Infrastructural Requirements and Regulatory Challenges of a Sustainable Urban Air Mobility Ecosystem. *Buildings* **2022**, *12*, 747. [CrossRef]
15. Li, Y.; Xie, Y.; Sun, S.; Hu, L. Evaluation of Park Accessibility Based on Improved Gaussian Two-Step Floating Catchment Area Method: A Case Study of Xi'an City. *Buildings* **2022**, *12*, 871. [CrossRef]
16. Ren, L.; An, F.; Su, M.; Liu, J. Exposure Assessment of Traffic-Related Air Pollution Based on CFD and BP Neural Network and Artificial Intelligence Prediction of Optimal Route in an Urban Area. *Buildings* **2022**, *12*, 1227. [CrossRef]
17. Zhao, Y.; Zhao, J. Numerical Assessment of Particle Dispersion and Exposure Risk in an Underground Parking Lot. *Energy Build.* **2016**, *133*, 96–103. [CrossRef]
18. Cui, S.; Xie, B.; Li, R.; Pei, J.; Tian, Y.; Zhang, J.; Xing, X. G-C_3N_4/CeO_2 Binary Composite Prepared and Its Application in Automobile Exhaust Degradation. *Materials* **2020**, *13*, 1274. [CrossRef]
19. Tobalina-Baldeon, D.; Sanz-Adan, F.; Martinez-Calvo, M.A.; Santamaría-Pena, J. Dynamic Tensile Stress-Compressive Stress Behavior of Thermoplastic Matrix Composite Materials Reinforced with Continuous Fiber for Automotive Damping and Anti-Vibration Structural Elements. *Materials* **2020**, *13*, 5. [CrossRef]

20. Zhao, Y.; Song, X.; Wang, Y.; Zhao, J.; Zhu, K. Seasonal Patterns of PM10, PM2.5, and PM1.0 Concentrations in a Naturally Ventilated Residential Underground Garage. *Build. Environ.* **2017**, *124*, 294–314. [CrossRef]
21. Nowoświat, A.; Dulak, L. Impact of Cement Dust Pollution on the Surface of Sound-Absorbing Panels on Their Acoustic Properties. *Materials* **2020**, *13*, 1422. [CrossRef]
22. Li, L.; Mullan, A.F.; Clements, N. Exposure to Air Pollution in Indoor Walkways of a Suburban City. *Build. Environ.* **2020**, *183*, 107171. [CrossRef]
23. Garcia, E.; Rice, M.B.; Gold, D.R. Air Pollution and Lung Function in Children. *J. Allergy Clin. Immunol.* **2021**, *148*, 1–14. [CrossRef]
24. Gamble, J.; Jones, W.; Minshall, S. Epidemiological-Environmental Study of Diesel Bus Garage Workers: Acute Effects of NO_2 and Respirable Particulate on the Respiratory System. *Environ. Res.* **1987**, *42*, 201–214. [CrossRef]
25. Zhang, W.; Li, Q.; Tang, M.; Zhang, H.; Sun, X.; Zou, S.; Jensen, J.L.; Liou, T.G.; Zhou, A. A Multi-Scale Approach to Study Biochemical and Biophysical Aspects of Resveratrol on Diesel Exhaust Particle-Human Primary Lung Cell Interaction. *Sci. Rep.* **2019**, *9*, 18178. [CrossRef]
26. Park, E.-J.; Roh, J.; Kang, M.-S.; Kim, S.N.; Kim, Y.; Choi, S. Biological Responses to Diesel Exhaust Particles (DEPs) Depend on the Physicochemical Properties of the DEPs. *PLoS ONE* **2011**, *6*, e26749. [CrossRef]
27. Jasevičius, R.; Kruggel-Emden, H.; Baltrėnas, P. Numerical Simulation of the Sticking Process of Glass-Microparticles to a Flat Wall to Represent Pollutant-Particles Treatment in a Multi-Channel Cyclone. *Particuology* **2017**, *32*, 112–131. [CrossRef]
28. Jasevičius, R.; Baltrėnas, P.; Kačianauskas, R.; Grubliauskas, R. DEM Simulation of the Impact of Ultrafine Glass Particles on the Partition Wall of the Multichannel Cyclone. *Part. Sci. Technol.* **2014**, *32*, 576–587. [CrossRef]
29. Jasevičius, R.; Tomas, J.; Kačianauskas, R. Simulation of Normal Impact of Ultrafine Silica Particle on Substrate. *Part. Sci. Technol.* **2011**, *29*, 107–126. [CrossRef]
30. Jasevičius, R. Numerical Modeling of the Mechanics of the Interaction of Coronavirus with the Lung Epithelial Cell. *Mech. Adv. Mater. Struct.* **2022**, *29*, 1–16. [CrossRef]
31. Park, K.; Kittelson, D.; Zachariah, M.; McMurry, P. Measurement of Inherent Material Density of Nanoparticle Agglomerates. *J. Nanoparticle Res.* **2004**, *6*, 267–272. [CrossRef]
32. Sen, N.; Weprin, S.; Peter, Y. Discrimination Between Lung Homeostatic and Injury-Induced Epithelial Progenitor Subsets by Cell-Density Properties. *Stem Cells Dev.* **2013**, *22*, 2036–2046. [CrossRef] [PubMed]
33. Roan, E.; Waters, C.M. What Do We Know about Mechanical Strain in Lung Alveoli? *Am. J. Physiol. Cell. Mol. Physiol.* **2011**, *301*, L625–L635. [CrossRef] [PubMed]
34. Jasevičius, R.; Baronas, R.; Kruggel-Emden, H. Numerical Modelling of the Normal Adhesive Elastic–Plastic Interaction of a Bacterium. *Adv. Powder Technol.* **2015**, *26*, 742–752. [CrossRef]
35. Fischer, H. Function of Proton Channels in Lung Epithelia. *Wiley Interdiscip. Rev. Membr. Transp. Signal.* **2012**, *1*, 247–258. [CrossRef]
36. Ng, A.W.; Bidani, A.; Heming, T.A. Innate Host Defense of the Lung: Effects of Lung-Lining Fluid PH. *Lung* **2004**, *182*, 297–317. [CrossRef]
37. Zasadzinski, J.A.; Stenger, P.C.; Shieh, I.; Dhar, P. Overcoming Rapid Inactivation of Lung Surfactant: Analogies between Competitive Adsorption and Colloid Stability. *Biochim. Biophys. Acta-Biomembr.* **2010**, *1798*, 801–828. [CrossRef]
38. Kang, D.; Chugunova, M.; Nadim, A.; Waring, A.J.; Walther, F.J. Modeling Coating Flow and Surfactant Dynamics inside the Alveolar Compartment. *J. Eng. Math.* **2018**, *113*, 23–43. [CrossRef]
39. Evans, J.A.; Whitelaw, W.A. The Assessment of Maximal Respiratory Mouth Pressures in Adults. *Respir. Care* **2009**, *54*, 1348–1359.
40. Lausted, C.G.; Johnson, A.T.; Scott, W.H.; Johnson, M.M.; Coyne, K.M.; Coursey, D.C. Maximum Static Inspiratory and Expiratory Pressures with Different Lung Volumes. *Biomed. Eng. Online* **2006**, *5*, 29. [CrossRef]